IOP Conf. Series: Journal of Physics: Conf. Series **1224** (2019) 012008 doi:10.1088/1742-6596/1224/1/012008

Numerical simulation of oil-water two-phase flow in a horizontal duct with a Venturi flow meter

M Guilizzoni, G Salvi, G Sotgia, L P M Colombo

Politecnico di Milano, Department of Energy, Via Lambruschini 4, 20156 Milano, Italy

E-mail: manfredo.guilizzoni@polimi.it

Abstract. The progressive depletion of on-shore and light-oil reserves is forcing an increased use of transitional and heavy oils, which implies new challenges both during the extraction and the transportation. Focusing on the latter, a technique to reduce the pressure drop is water injection in the oil stream to create the so-called core annular flow (CAF), a flow regime with an oil core enveloped in a water annulus wetting the pipe wall, so that the apparent viscosity of the mixture is considerably reduced. Behaviour of CAF in ducts with non-uniform sections is still under research. This work is devoted to a CFD investigation about the pressure drop, pressure gradients, velocity profiles and *in situ* volume fractions in a duct including a Venturi flow meter. Unsteady RANS simulations were carried out using the Volume-Of-Fluid *interFoam* solver of OpenFOAM. Numerical results were experimentally validated for oil superficial velocities in the range 0.25–0.75 m/s and water superficial velocities in the range 0.44–1.10 m/s and comparisons between different approaches and sensitivity analyses were performed. Satisfactory agreement was found for the pressure drop and pressure gradients, and also for the *in situ* volume fraction with respect to the predictions of the Arney correlation.

1. Introduction

A large majority of the world energy demand is nowadays still satisfied by oil, and since the last decades progressive depletion of on-shore and light-oil reserves forced an increased use of transitional and unconventional/heavy oils. These are available in a larger total amount and in a higher number of countries, but also pose new challenges. In fact, despite different classifications, they share the main characteristic of having higher densities, viscosities, sulfur and impurities contents than the conventional oil, so that they that cannot be extracted, transported and processed using conventional techniques [1, 2]. In particular, pipeline transport of unconventional/heavy oils is problematic due to their high densities and particularly high viscosities. Among the possible solution to make it feasible, the creation of a peculiar two-phase flow pattern, in which the apparent viscosity is reduced, is at present under study and development [3]. Such a flow pattern is named Core Annular Flow (CAF): an oil core flows in the central part of the pipeline, while a "lubricating" water annulus wets the duct wall [4-6], thus reducing the wall shear stress and lowering the pressure drop. This favorable flow pattern only occurs for suitable velocities of the phases, so it is very important to measure and/or to predict the mass flow rates of the phases and of the total mixture. Moreover, the stability of Core Annular Flow in presence of variations in the pipeline (e.g. bends, changes in the cross-section, in-line measurement devices) is still under investigation.

This paper is therefore devoted to a Computational Fluid Dynamics (CFD) study aimed at characterizing the flow of an oil-water mixture in the Core Annular Flow regime within a pipeline section including a Venturi flow meter. Such a computational domain offers the opportunity to get information about the flow behavior both along straight ducts (upstream and downstream) and within a measurement device whose converging/diverging profile also represents a reduction and an expansion of the flow cross-section. Moreover, such a device can be of great practical interests for the oil and gas industry because it has no moving parts, thus greatly reducing the need for maintenance [7]; but an issue in its use is that it is necessary to rely on models to correlate the measured pressure difference to the mass flow rates. Thus, accurate characterization of the multiphase flow across it is needed.

2. Literature review

Even if the literature is not as vast as for gas-liquid flows, nowadays many papers can be found about liquid-liquid oil-water flows. Reference to many of the most important papers about this topic can be found in [8]. Focusing the attention on Core Annular Flow, pioneering studies were performed by Charles [9], followed (in a not exhaustive list) by Ooms et al [10], Oliemans et al. [11], Brauner [12], Arney et al. [13], Joseph et al. [6], Angeli and Hewitt [14], Sotgia et al. [6], Colombo et al. [15], Colombo et al. [16]. A review can be found in the book by Joseph and Renardy [17].
Concerning the numerical simulation of two-phase flows and particularly of oil-water flows, simplified (e.g. one-dimensional) models are implemented also in commercial software commonly used by companies in the oil and gas sector (e.g. OLGA Dynamic Multiphase Flow Simulator [18]). On the contrary, reliable three-dimensional simulations are still an open research problem and only a minor number of papers are available in the literature [19-21]. The work by Babakhani Dehkordi et al [21], focused on the flow within a Venturi meter, also includes a review about measurement devices used for two-phase and particularly oil-water flows.

3. Numerical model

3.1. Volume-Of-Fluid in interFoam

In the Core Annular Flow pattern, two immiscible phases are separated by an interface having a length scale comparable to the pipe diameter (particularly for the oil core, but also for the oil drops if present). Such interface is continuously varying in terms of shape and extension, due to the evolution of the flow structures, including also possible breakup and coalescence. The two phases can be both approximated to incompressible. One of the most suitable CFD approaches for similar scenarios is the Volume-Of-Fluid (VOF), introduced by Hirt and Nichols [22]. The latter was originally developed for different two-phase applications (e.g. drop impacts), but examples of their use for two-phase flow are already reported in the literature [19, 20, 23]. More complex methods could also be used (e.g. [24]), but no ready-to-use solver is available, so at present their use is practically restricted to academic studies. On the contrary, the aim of this paper is to investigate the performances of an open source software package when used in "field" conditions, i.e. with common hardware, an intermediate knowledge about CFD and requiring reasonably short simulation times. Therefore, VOF was selected for this study and simulations were performed on 3D domains using the *interFoam* solver of the OpenFOAM open source CFD toolbox. OpenFOAM was selected due to its free and open source nature and to the many favourable reviews and successful cases of use described in the literature (e.g. see references 13-17 in [25]). *interFoam* is an isothermal finite volume solver implementing a modified version of the VOF model, with the continuum surface force (CSF) model to include surface tension at the interface [26]. It solves a single set of equations, constituted by the usual mass and momentum conservation equations for incompressible flow, plus an additional equation for the *in situ* volume fraction γ (i.e. the ratio between the volume occupied by one phase and the total volume in a certain domain region) that is transported by the fluid velocity field w:

$$\partial\gamma / \partial\tau + \nabla\cdot(\mathrm{w}\,\gamma) + \nabla\cdot[\mathrm{w_r}\,\gamma\,(1-\gamma)] = 0 \qquad (1)$$

As it can be noticed from Eq. 1, *interFoam* introduces an additional term in the volume fraction equation with respect to the original VOF model. In this term, w_r is the "compression velocity" that is obtained by multiplying the maximum velocity magnitude in the transition region (i.e. the region where $0 < \gamma < 1$) by the normal to the interface vector and by an adjustable coefficient. Thanks to the additional term, which is active only in the interfacial region, the latter is compressed to very few cells. *interFoam* performs volume tracking and interface reconstruction, with no explicit interface tracking, so parasitic velocities due to spurious capillary effects [27] may arise. On macroscopic domains as those studied in this work, this is not an issue. Further details about *interFoam* can be found in [28].

3.2. Fluid properties and turbulence models

Both oil and water were assumed as Newtonian and incompressible fluids. Density and viscosity were set for oil at ρ_o = 890 kg/m^3 and μ_o = 0.830 Pa s respectively, and for water at ρ_w = 1000 kg/m^3 and $\mu_w = 1.026 \times 10^{-3}$ Pa s respectively, corresponding to the values in the experiments used for validation.
At the investigated velocities of the phases, flow is laminar in the oil core and turbulent in the water annulus. As the VoF method models a single fictitious fluid, it is not possible to consider the two phases separately; so unsteady Reynolds-Averaged Navier-Stokes (RANS) simulations were performed for the whole fluid domain. The k-ε turbulence model, with standard wall functions and values for the involved constants, was selected as a first choice for the simulations. Additional simulations were also performed with the k-ω Shear Stress Transport model. Details about the two models can be found in Versteeg and Malalasekera [29].

3.3. Discretization schemes and CFL settings

The implicit Euler scheme (first-order accurate) was used to discretize the time derivative. The Gauss linear scheme was used for the gradient terms, while the Gauss linear corrected scheme for the Laplacian terms. For the divergence terms, Gauss upwind was used for the velocity and the turbulence variables, Gauss van Leer and Gauss linear or *interfaceCompression* (a peculiar scheme of OpenFOAM for the compression velocity) for the volume fraction.
The PISO (Pressure Implicit with Splitting of Operators) algorithm was used to deal with the pressure-velocity coupling. The linear solver PCG (preconditioned conjugate gradient) with a DIC (Diagonal Incomplete-Cholesky) preconditioner was selected for pressure, while the linear *smoothSolver* with a symmetric Gauss Seidel smoother for all the other variables. Some volume fraction sub-cycles were also performed. The maximum allowed Courant–Friedrichs-Lewy (CFL) number was set to 0.3 (sensitivity analysis was then performed raising it to 0.5): the solver is let free to adapt the time step to keep the CFL number under this desired limit (that is the requirement for the interface compression scheme used in *interFoam* for 3D cases)

3.4 Domain, mesh and boundary conditions

Figure 1 shows a sketch of the simulation domain and mesh (coarsened for better visualization) with an example of results in terms of shape of the oil core and of velocity field on the duct axial vertical plane. Boundary conditions for the different variables are also summarized. The insets show a cross-sectional view of the mesh and an example of the oil core shape observed in the Venturi flow meter during the experiments.
The simulated domain includes a section of a pipeline with 40 mm i.d., equipped with a Venturi flow meter (designed according to the ISO standards) having a 30 mm i.d. throat and a total length of 120 mm (35 mm before the throat and 85 mm after the same). Three domains, differing in the lengths of the upstream and downstream pipes, were tested:

- domain A: upstream duct 200 mm, downstream duct 150 mm;
- domain B: upstream duct 500 mm, downstream duct 150 mm;
- domain C: upstream duct 600 mm, downstream duct 200 mm;

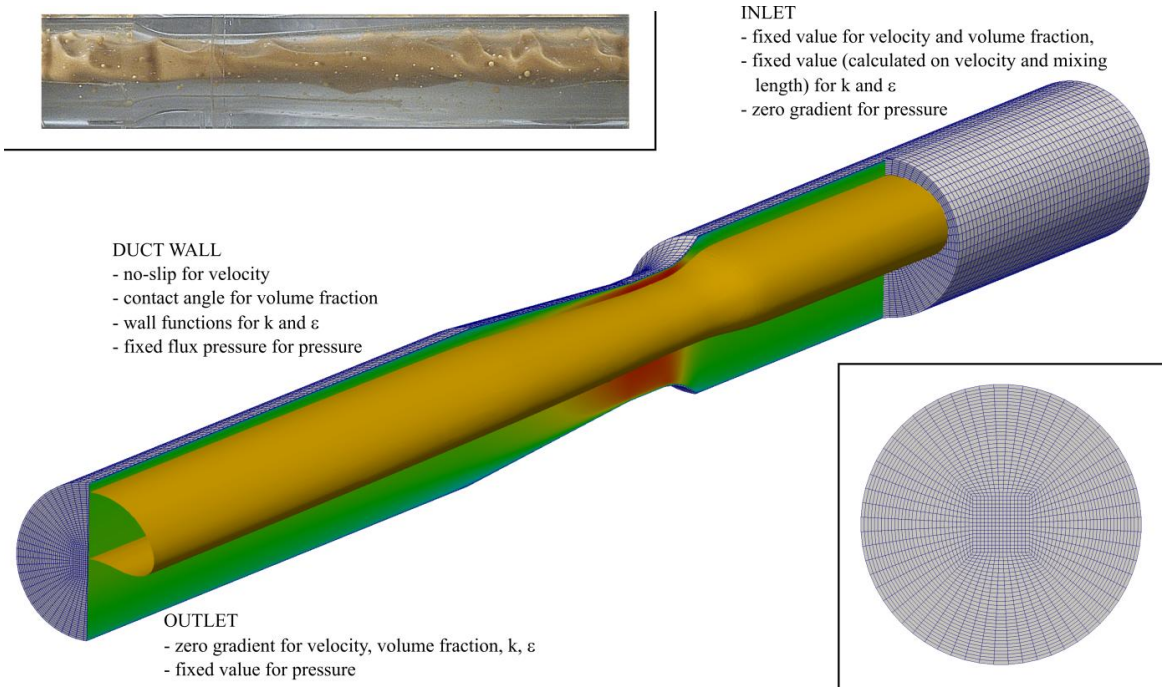

Figure 1. Sketch of the investigated domain and mesh (coarsened for better visualization) with an example of results in terms of shape of the oil core and velocity field along the duct axial vertical plane. In the insets: an example of the oil core shape observed in the Venturi flow meter during the experiments and a cross-sectional view of the used mesh.

Shorter lengths obviously affected negatively the determination of the distributed pressure drop, so the three domains were selected as a compromise between this aspect and the computational effort.
The meshes – in all cases structured – were created by the *blockMesh* OpenFOAM utility. Different mesh refinements were used to test mesh independence. The latter is always an issue when using the VOF approach and for the situation under study it was expected to be problematic due to the presence of the water annulus, which for some flow conditions is quite thin towards the top part of the duct. Strict mesh independence was not reached, but the following meshes were selected, again as a reasonable compromise between the mesh sensitivity and the computational effort:

- coarse mesh used for domain A: 143k cells;
- coarse mesh used for domain B: 233k cells;
- fine mesh used for domain C: 747k cells.

The values are relatively low, but they must be evaluated considering that transient simulations were performed and that the oil core – entering the domain at the inlet – had to move across the whole domain and then to reach a pseudo-steady configuration. With these domains and meshes the simulation time was in the range 15-30 hours (depending on the phase velocities) for cases A and B and between 80 and 140 hours for case C, on desktop/laptop computers equipped with Intel i5 and i7 series processors. A different choice might have been to initialize a certain shape of the oil core along the whole domain and to let it reach its equilibrium structure, possibly using a modified version of *interFoam* that is able to use local time stepping (*LTSInterFoam*) to make convergence towards pseudo steady-state conditions faster.
For all cases, mesh quality was checked in terms of aspect ratio, skewness and orthogonality.

A side-effect of using a mesh that is quite coarse near the wall is that for some cases the oil sticks to the wall for flow conditions in which experimentally this is not observed. As it will be discussed in Section 6, to solve this issue the duct wall was modelled as super-hydrophilic. This is why in Table 1 some cases are referred to as "standard wall" (zero-gradient boundary condition for the volume fraction, i.e. contact angle for a water drop in a surrounding oil ambient equal to 90°) and others as "hydrophilic wall" (contact angle for a water drop in a surrounding oil ambient equal to 3°).
Initial conditions of the two phases and the position and shape of the oil inlet were set using the *setFields* and *snappyHexMesh* OpenFOAM utilities.

4. Experimental set-up, procedures and results

The numerical results were validated against experimental data obtained during previous campaigns. Details about the experimental setup, procedure and results that were used for the validation can be found in [6, 30, 31].

5. Investigated flow conditions and setting of the inlet boundary conditions

Among the available experimental flow conditions, eight representative cases were selected for the CFD analysis, with superficial and actual velocities of oil and water as reported in Table 1. All of them show a Core Annular Flow pattern.
The Arney correlation [13] was used to estimate the *in situ* volume fractions at the duct inlet. Such fractions were in turn used to split the inlet section into two parts – cells belonging to the oil core and cells belonging to the water annulus – and to set the cross-sectional averaged effective phase velocities as boundary conditions for the velocity in the two regions.
Concerning the subdivision of the inlet between oil and water, in addition to the area also the shape of the two regions has to be decided. A basic choice is to use a circle centered on the axis for the oil and a circular crown for the water, but this neglects the effect of buoyancy. So also different choices in terms of shapes and position of the oil inlet were tested, as it will be discussed in Section 6.
In terms of implementation, the oil and water inlet regions were set using the *blockMesh* and *snappyHexMesh* OpenFOAM utilities.

6. Result and Discussion

6.1. Pressure drop and pressure gradients

Preliminary simulations about single-phase water flow within the domain showed excellent agreement with the predictions of the classic theory about pressure drop along the constant-section ducts and within the Venturi flow meter, both in laminar and turbulent conditions.
For the two-phase flow simulations, Table 1 summarizes the majority of the obtained numerical results and their comparison with the experimental data, in terms of:

- pressure drop in the Venturi flow meter (calculated as the difference between the pressure immediately before the device and the pressure at the throat);
- pressure gradient in the upstream duct;
- pressure gradient in the downstream duct.

Additional cases, whose results showed no significant difference from the ones reported, are omitted in the table and will only be commented hereinafter.
As already said, the investigated flow conditions are identified in terms of superficial velocities of the phases J and of cross-sectional averaged actual velocities at the inlet w.
In the first case (DA-CM-NW-GL), the upstream and downstream ducts proved to be too short for a reliable calculation of the pressure gradients, as their lengths are not sufficient for the flow to develop after the inlet region and re-develop after the Venturi flow meter. Nevertheless, the pressure drop in the latter is already captured with discrete accuracy: on the eight investigated cases, the mean absolute percentage error (MAPE) is around 16 %.

Table 1. Investigated flow conditions and comparison between the numerical and experimental results for: a) Venturi pressure drop, b) pressure gradient in the upstream duct, c) pressure gradient in the dowstream duct.

DA-CM-NW-GL Domain A, coarse mesh, standard wall, "Gauss linear" scheme for γ
DB-CM-NW-GL Domain B, coarse mesh, standard wall, "Gauss linear" scheme for γ
DB-CM-HW-GL Domain B, coarse mesh, hydrophilic wall, "Gauss linear" scheme for γ
DB-CM-HW-IC Domain B, coarse mesh, hydrophilic wall, "Interface compression" scheme for γ
DC-FM-HW-GL Domain C, fine mesh, hydrophilic wall, "Gauss linear" scheme for γ

Case	J [m/s]		w [m/s]		Venturi pressure drop [kPa]						PE [-]				
	Oil	Water	Oil	Water	EXP	DA-CM-NW-GL	DB-CM-NW-GL	DB-CM-HW-GL	DB-CM-HW-IC	DC-FM-HW-GL	DA-CM-NW-GL	DB-CM-NW-GL	DB-CM-HW-GL	DB-CM-HW-IC	DC-FM-HW-GL
1	0.25	0.44	0.89	0.62	0.56	0.52	0.52	0.52	0.52	0.52	-7.1	-7.1	-7.1	-7.1	-7.1
2	0.46	0.44	1.09	0.77	1.04	0.86	0.88	0.86	0.88	0.87	-17.3	-15.4	-17.3	-15.4	-16.3
3	0.52	0.67	1.47	1.03	2.11	1.46	1.47	1.47	1.48	1.48	-30.8	-30.3	-30.3	-29.9	-29.9
4	0.64	0.67	1.60	1.12	2.06	1.78	1.80	1.80	1.81	1.82	-13.6	-12.6	-12.6	-12.1	-11.7
5	0.64	0.89	1.92	1.33	2.74	2.45	2.43	2.43	2.43	2.47	-10.6	-11.3	-11.3	-11.3	-9.9
6	0.64	1.10	2.24	1.55	3.50		3.19	3.19	3.18	3.22		-8.9	-8.9	-9.1	-8.0
7	0.75	0.67	1.70	1.20	2.19		2.10	2.09	2.10	2.12		-4.1	-4.6	-4.1	-3.2
8	0.75	0.89	2.02	1.41	2.93		2.79	2.79	2.78	2.82		-4.8	-4.8	-5.1	-3.8
										MAPE [-]	15.9	11.8	12.1	11.8	11.2

Case	J [m/s]		w [m/s]		Upstream pressure gradient [kPa/m]						PE [-]				
	Oil	Water	Oil	Water	EXP	DA-CM-NW-GL	DB-CM-NW-GL	DB-CM-HW-GL	DB-CM-HW-IC	DC-FM-HW-GL	DA-CM-NW-GL	DB-CM-NW-GL	DB-CM-HW-GL	DB-CM-HW-IC	DC-FM-HW-GL
1	0.25	0.44	0.89	0.62	0.05										
2	0.46	0.44	1.09	0.77	0.14										
3	0.52	0.67	1.47	1.03	0.31		0.38	0.38	0.38	0.39		22.4	22.4	22.1	26.0
4	0.64	0.67	1.60	1.12	0.38		0.45	0.45	0.45	0.46		18.4	18.4	18.0	19.9
5	0.64	0.89	1.92	1.33	0.52		0.59	0.59	0.58	0.59		12.5	12.5	10.4	12.2
6	0.64	1.10	2.24	1.55	0.67		0.74	0.74	0.73	0.73		9.2	9.2	8.1	8.8
7	0.75	0.67	1.70	1.20	0.44		0.52	0.52	0.51	0.52		18.0	17.9	16.2	18.1
8	0.75	0.89	2.02	1.41	0.61		0.66	0.66	0.64	0.66		7.9	7.9	5.5	8.8
										MAPE [-]		14.7	14.7	13.4	15.6

Case	J [m/s]		w [m/s]		Downstream pressure gradient [kPa/m]						PE [-]				
	Oil	Water	Oil	Water	EXP	DA-CM-NW-GL	DB-CM-NW-GL	DB-CM-HW-GL	DB-CM-HW-IC	DC-FM-HW-GL	DA-CM-NW-GL	DB-CM-NW-GL	DB-CM-HW-GL	DB-CM-HW-IC	DC-FM-HW-GL
1	0.25	0.44	0.89	0.62	0.07										
2	0.46	0.44	1.09	0.77	0.17										
3	0.52	0.67	1.47	1.03	0.31		0.74	0.26	0.36	0.31		141.0	-16.8	17.8	-0.1
4	0.64	0.67	1.60	1.12	0.39		0.79	0.33	0.55	0.37		102.7	-16.5	40.0	-4.1
5	0.64	0.89	1.92	1.33	0.50		0.39	0.37	0.53	0.45		-23.0	-27.2	4.9	-10.1
6	0.64	1.10	2.24	1.55	0.64		0.43	0.43	0.44	0.53		-33.9	-33.9	-31.3	-17.0
7	0.75	0.67	1.70	1.20	0.51		0.43	0.37	0.50	0.43		-16.1	-28.5	-3.5	-17.4
8	0.75	0.89	2.02	1.41	0.62		0.42	0.42	0.45	0.50		-31.9	-32.1	-27.5	-18.4
										MAPE [-]		58.1	25.8	20.8	11.2

The accuracy in the prediction of the concentrated pressure drop in the Venturi flow meter is improved when using the longer domains, with a reduction of the MAPE to around 12 % for domain B and to around 11 % for domain C. Given the domain, different settings (hydrophilic wall, Gauss linear or *interfaceCompression* schemes for the volume fraction, different shapes for the oil inlet, variations in the inlet boundary conditions for the main variables) cause practically no difference in the results. So it can be concluded that the prediction of the concentrated pressure drop in the Venturi meter is quite robust.

Concerning the pressure gradients, for the upstream duct the different investigated domains (B and C), mesh types and wall wettability (standard or hydrophilic wall) cause practically no difference. Slight improvement is offered by the use of the *interfaceCompression* scheme instead of the Gauss linear scheme for the volume fraction. The most significant observation is that the accuracy of the simulation is quite different between the investigated flow conditions. The numerical simulations always overestimate the experimental values, but no significant trend (e.g., improving/worsening of the prediction for increasing/decreasing phase velocities) could be identified.

Overall, the MAPE is around 14-15 % which in any case can be considered as satisfactory. For comparison, the uncertainties in the estimation of the two-phase pressure gradient when using experimental models and correlations usually reach much more than 20 %.

For the downstream duct, in two cases (case 3 and case 4 in Table 1) the oil touched the duct wall, while in the corresponding experimental tests Core Annular Flow without oil fouling was observed. This is due to the fact that for those cases, at low phase velocities, the buoyancy effect is more significant and the top part of the water annulus is very thin, so that the mesh is too coarse to keep oil away from the wall. To overcome this problem without being forced to refine the mesh, the wettability of the duct surface was modified in the simulations, changing the value of the contact angle in the volume fraction boundary condition from 90° to 3°, i.e. a super-hydrophilic surface was artificially set. This effectively prevents the oil from sticking to the wall and the results become more reliable. As the domain dimensions are such that capillary effects are negligible, this unrealistic boundary condition should have no influence on the simulations for all the cases in which water is correctly in contact with the duct wall. Comparison of the DB-CM-NW-GL and DB-CM-HW-GL columns in Table 1 a, b, c confirms this hypothesis: results for the Venturi pressure drop and upstream pressure gradient are practically identical, and only the downstream cases in which the oil with the DB-CM-NW-GL settings was touching the duct wall show a changed value.

Still focusing the attention on the downstream duct, it can be seen that in this case the choice of the discretization scheme for the volume fraction and the use of domains B and C imply a significant difference in the results.

Overall, the use of the *interfaceCompression* scheme offers an improvement, even if an even better improvement is given by the use of the longer domain C with a finer mesh.

With the latter, the MAPE is as low as 11 %, which once again can be considered as a very satisfactory value, particularly considering that for case DC-FM-HW-GL the results show a more consistent trend: they always underestimate the experimental results, with an error that increases for higher velocities of the phases (but still remaining under 20 %).

Further tests, not reported in Table 1, were also performed to investigate the effects of:

- a variation in the maximum admitted Courant number. The latter was increased to 0.5 with no effect on the results;
- variations in the values of the initial velocity field in the duct (still or already flowing water), of the turbulent kinetic energy and its dissipation rate, of the turbulent viscosity, of the oil viscosity (that was reduced of 20 %). All these factors were varied independently, leading to changes in the results lower than 1 %. In the case of the oil viscosity this may seem surprising, but it is physically correct because in a Core Annular Flow only water is in contact with the duct wall and thus experiences the vast majority of the friction;
- a change in the shape of the oil and water region at the duct inlet. Oil cores shaped as a circle centered on the duct axis, as an eccentric half-circle, ellipse or half-moon region were tested.

No effect was observed on the Venturi pressure drop, while the pressure gradients showed minor differences, but with no indication that a certain shape is the best choice;

- the use of the *k-ω* SST turbulence model instead of the *k-ε* model. Motivation for this additional test is the fact that the *k-ε* model was used with the standard wall functions, but in some cases the *y+* values are partially out from the correct range for use of the wall functions themselves. The average *y+* value for domain B with coarse mesh is around 28, and when using the fine mesh the value obviously becomes lower. Using coarser meshes near the duct wall would worsen the description of the water annulus and increase the risk of spurious oil fouling. So case 7 of Table 1 was tested with the DB-CM-HW-GL settings and the *k-ω* SST turbulence model. Contrarily to what was expected, results were worse than with the *k-ε* model, with errors equal to 13.2 % upstream and 52.2 % downstream. Further investigation about this aspect is therefore needed, also using further refined meshes that can be more suitable for the *k-ω* model.

6.2. In situ volume fraction

In addition to analysing the pressure evolution along the flow, the velocity profiles and the *in situ* volume fractions of the phases can be extracted from the simulation results to study the flow structure. Of particular interest for comparison with simplified 1D models and experimental correlations is the analysis of the cross-sectional averaged *in situ* volume fractions *H*, that can be also related to the slip ratio between the phase velocities. Figure 2 shows the results for the *in situ* volume fractions of water H_w for three different positions along the duct axis, compared to the predictions of the homogeneous model and of the Arney correlation [13]:

$$H_w = \varepsilon_w [1 + 0.35 (1 - \varepsilon_w)] \quad (2)$$

where ε_w is the water volume ratio, i.e. the ratio between the water volume flow rate and the total volume flow rate at the duct inlet.

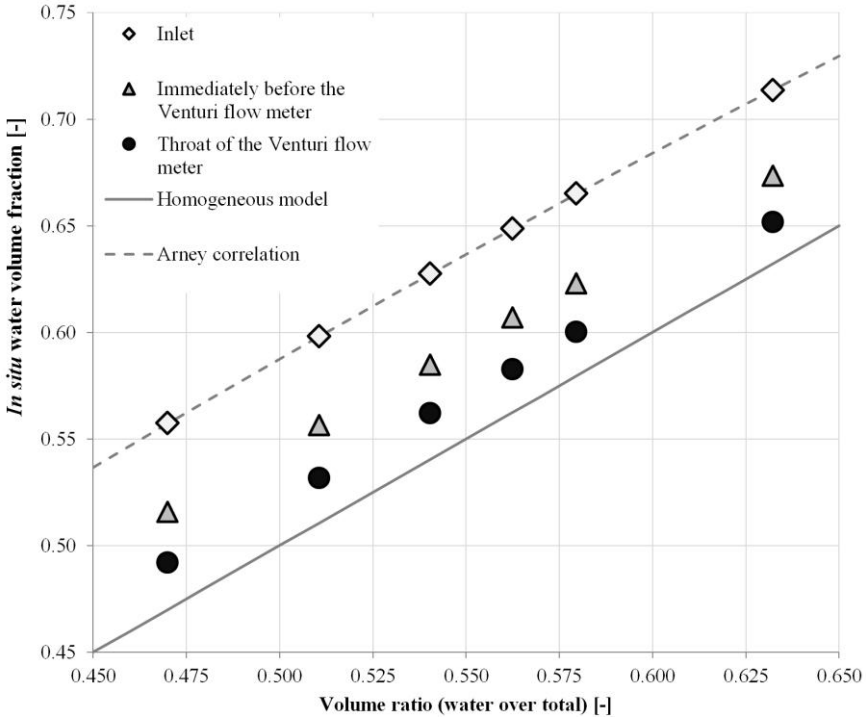

Figure 2. *In situ* water fraction calculated from the numerical simulations, compared to the predictions of the homogeneous model and the Arney correlation.

At the inlet the values are obviously superposed to the latter, as it was such a correlation to be used to set the oil and water regions. Then an evolution occurs and at the Venturi flow meter throat the values are much nearer to the predictions of the homogeneous model, confirming previous results both experimental [31] and numerical [21]. As already reported in [21] this should be related to the fact that in the Venturi water accelerates more than oil (due to the higher viscosity of the latter), so that the difference between the phase velocities is reduced. This also allows using the Venturi flow meter for the determination of the flow rates of the phases [31][32].

7. Conclusions

The performed CFD simulations evidenced that the *interFoam* solver of OpenFOAM allows predicting the pressure drop of oil-water two-phase flows along straight pipes and within a Venturi flow meter with good accuracy. With the used domains and settings, the deviations with respect to experimental data, in terms of MAPE, are within 11-12 % for the concentrated pressure drop, around 14-15 % for the pressure gradient upstream of the Venturi flow meter and around 11 % downstream of the same. Simulations can be performed on a common personal computer in a reasonably short time. Results are quite robust with respect to the settings of the inlet conditions, in terms both of cross-sectional shape of the inlet regions for the two phases and of boundary conditions for the turbulence variables, and the oil physical properties. Prediction of the pressure drop within the Venturi flow meter is also very robust with respect to the length of the investigated domain; pressure gradients along the upstream and downstream ducts are on the contrary more sensitive to the latter variable. A very good agreement was additionally found between the calculated *in situ* volume fractions and the predictions of the Arney correlation. As some investigated cases showed much larger errors (up to 30%) and the use of the k-ω SST model with respect to the k-ε model implied significantly different results, further studies are needed to investigate the modeling options more thoroughly.

8. Nomenclature

H	*in situ* volume fraction (-)
J	superficial velocity (m/s)
k	turbulent kinetic energy (J/kg)
MAPE	mean absolute percentage error (%)
PE	percentage error (%)
w	actual velocity (m/s)

Greek Symbols

ε	volume ratio (-)
ε	turbulent dissipation (J/kg-s)
γ	volume fraction for the VoF method (-)
μ	dynamic viscosity (Pa s)
ρ	density (kg/m^3)
τ	time (s)
ω	turbulence specific dissipation rate (1/s)

Subscripts and superscripts

o	oil
w	water

References

[1] IEA International Energy Agency 2013 *Resources to Reserves 2013* (available online at: http://www.iea.org/publications/freepublications/publication/Resources2013.pdf)
[2] Gordon D 2012. Understanding Unconventional Oil *The Carnegie papers, Energy and climate* (available online at: http://carnegieendowment.org/files/unconventional_oil.pdf)
[3] Saniere A, Hénaut I, Argillier J F 2004 *Oil & Gas Science and Technology – Rev. IFP* **59**(5) 455–66
[4] Oliemans R, Ooms G 1986 Core annular flow of oil and water through a pipeline. In: Hewitt G F, Delhaye J M, Zuber N (Eds.) *Multiphase Science and Technology* (Hemisphere Publishing Corp., Washington) **2**
[5] Joseph D, Bai R, Chen K P and Renardy R 1997 *Annu. Rev. Fluid Mech.* **29** 65–90
[6] Sotgia G, Tartarini P and Stalio E 2008 *Int. J. Multiphas. Flow* **34** 1161–74

[7] Atkinson I et al 2004/2005 A New Horizon in Multiphase Flow Measurement. (available online at: http://www.slb.com/resources/publications)
[8] Wang W, Gong J, Angeli P 2011 *Int. J. Multiphas. Flow* **37** 1156–64
[9] Charles M E, Govier G W and Hodgson G W 1961 *Can. J. Chem. Eng.* **39**(1) 27–36
[10] Ooms G, Segal A, Van Der Wees A J, Meerhoff R and Oliemans R V A 1984 *Int. J. Multiphas. Flow* 10 41–60
[11] Oliemans R V A, Ooms G, Wu H L and Duijvestijn A 1987 *Int. J. Multiphas. Flow* **13**(1) 23–31
[12] Brauner N 1991 *Int. J. Multiphas. Flow* **17**(1) 59–76
[13] Arney M S, Bai R, Guevara E, Joseph D D and Liu K 1993 *Int. J. Multiphas. Flow* **19**(6) 1061–76
[14] Angeli P, Hewitt G F 2000 *Int. J. Multiphas. Flow* 26 1117–40
[15] Colombo L P M, Guilizzoni M and Sotgia G M 2012 *Exp. Fluids* **53** 1617–25
[16] Colombo L P M, Guilizzoni M, Sotgia G M and Marzorati D 2015 *Int. J. Heat Fluid Fl.* **53** 91–97
[17] Joseph D, Renardy Y 1993 *Fundamentals of Two-Fluid Dynamics* (Springer, New York US)
[18] OLGA Dynamic Multiphase Flow Simulator (available online at: https://www.software.slb.com/products/olga)
[19] Ghosh S, Das G and Das P K 2010 *J. Chem. Eng. Process* **49** 1222–28
[20] Kaushik V V R, Ghosh S, Das G and Das P K 2012 *J. Pet. Sci. Eng.* **86–87** 153–64
[21] Babakhani Dehkordi P, Colombo L P M, Guilizzoni M and Sotgia G M 2017 *J. Pet. Sci. Eng.* **149** 540–52
[22] Hirt C W, Nichols B D 1981 J. Comp. Phys. **39**(1) 201–25
[23] Desamala A B, Vijayan V, Dasari A, Dasmahapatra A K and Mandal T K 2016 *J. Hydrodyn. Ser. B* 28 (4) 658–68
[24] Menard T, Tanguy S and Berlemont A 2007 *Int. J. Multiphas. Flow* **33**(5) 510–24
[25] Guilizzoni M, Santini M, Lorenzi M, Knisel V, Fest-Santini S 2014 *J. Phys.: Conf. Ser.* **547** 012028
[26] Brackbill J U, Khote D B and Zemach C 1992 *J. Comput. Phys.* **100**(2) 335–354
[27] Harvie D J E, Davidson M R and Rudman M 2006 *Appl. Math. Model.* **30** 1056–66
[28] Deshpande S S, Trujillo M F, Wu X and Chahine G 2012 *Int. J. Heat Fluid Flow* **34**(1) 1–14
[29] Versteeg H K, Malalasekera W 2007 *An Introduction to Computational Fluid Dynamics: The Finite Volume Method* (Pearson)
[30] Colombo L P M, Guilizzoni M, Sotgia G M, Babakhani Dehkordi P and Lucchini A 2017 *J. Phys.: Conf. Ser.* **923** 012012
[31] Colombo L P M, Guilizzoni M, Sotgia G M 2017 *Proc. 14th Int. Conf. on Multiphase Flow in Industrial Plant*, Desenzano del Garda (Brescia), Italy, Sept. 13 – 15, 2017
[32] Patent request Nr 102017000025126, "Procedimento e dispositivo per la misura delle portate dei componenti non miscibili di un flusso bifase liquido-liquido, Ministero dello Sviluppo Economico, 2017/03/07.